Integrating white matter anisotropy and structural connectivity for enhanced electric field precision in tDCS: a computational study

G. Caiani[1,2], E. Arrigoni[3], E. Chiaramello[2], M. Parazzini[2], A. Pisoni[3] and S. Fiocchi[2]
[1] *DEIB Politecnico di Milano, Piazza Leonardo da Vinci 32, Milano 20133, Italy*
[2] *CNR Consiglio Nazionale delle Ricerche - IEIIT, Piazza Leonardo da Vinci 32, 20133 Milano, Italy*
[3] *Department of Psychology, University of Milano-Bicocca, P.za Ateneo Nuovo 1, Milano, Italy*

***Abstract*—Transcranial direct current stimulation (tDCS) is a non-invasive brain stimulation technique with promising application in the treatment of neurological and psychiatric disorders. However, its efficacy is hindered by inter-subject variability in aftereffects, mainly due to anatomical differences across subjects which are not considered during protocol design. Among these, structural connectivity plays a crucial role but remains underexplored in tDCS research.**

This study advances tDCS modelling by integrating white matter anisotropy into finite element method (FEM) simulations to assess how structural connectivity variations influence electric field (EF) distribution. By combining advanced computational approaches, we explore the relationship between EF strength and cortical connectivity, offering new insights into the subject-specific effects of tDCS. Incorporating white matter anisotropy altered EF distribution in the most connected regions to the anodal stimulation site, affecting its intensity, direction, and spread. Preliminary findings also suggest a positive and significant ($p<0.05$) correlation between EF focality and the strength of connectivity between cortical areas P2 and C2.

***Keywords*—brain stimulation, electromagnetic simulation, white matter anisotropy, structural connectome.**

I. Introduction

TRANSCRANIAL Direct Current Stimulation (tDCS) is a non-invasive brain stimulation technique that delivers a weak constant current through scalp-mounted electrodes [1], generating electric fields (EF) that modulate spontaneous neuronal firing rate, inducing plasticity [2]. This mechanism makes tDCS a promising neuromodulation tool [3], with applications in different neuropsychological and psychiatric disorders [4].

However, its clinical applicability remains limited by significant intersubject variability in aftereffects, likely due to differences in EF distributions across subjects [5]. Anatomical quantities, such as skull thickness, cerebrospinal fluid, scalp-to-cortex distance, gyral and sulcal anatomy, age, and sex contribute to such variability [6], highlighting the need for personalised tDCS protocols.

Computational studies have improved tDCS modelling by incorporating subject-specific MRI-derived models, but most of them rely on isotropic tissue compartment models, neglecting white matter anisotropy. Structural connectivity, a key factor in intersubject variability [7], influences individual responsiveness to tDCS. Diffusion tensor imaging (DTI) enables the modelling of white matter pathways revealing subject-specific neural connections [8]. However, integrating white matter anisotropy into personalized models remains a challenge, with a few studies addressing its impact on EF distributions. Though, they mainly focus on the topology of the EF distribution [9] [10] [11] rather than its relationship with structural connectivity.

A major challenge in connectome-based studies is the lack of consensus on the best methodology for quantitative tractography analysis [12]. The most common used metric, fibre tract count, does not accurately reflect the underlying axonal density. Smith et al [13] have suggested algorithms, such as spherical-deconvolution informed filtering of tractograms (SIFT2), to increase this biological plausibility.

In this context, this study aims to advance the understanding of how structural connectivity differences across subjects affect the EF distribution in specific areas. Furthermore, it seeks to evaluate whether this distribution can be correlated with the strength of connections between cortical regions. This aim was reached through computational approaches, by combining cutting-edge methodologies to integrate white matter anisotropy in FEM simulations and to evaluate the subject specific connectome metrics.

II. Materials and Methods

A. Participants and data acquisition

Participants. Sixteen healthy, right-handed volunteers (nine males, mean age 23.5 ± 3.4 years) participated in the study. All participants gave written informed consent prior to their involvement. The study was conducted in the RM3T laboratory of the University of Milano-Bicocca in accordance with the declaration of Helsinki and the approval of the local Ethics Committee.

Data acquisition. The anatomical T1-weighted MRI and diffusion weighted (DW) images were acquired on a 3T Philips Ingenia CX MRI scanner. T1w structural images were obtained using a 3D magnetization-prepared gradient-echo sequence (TR = 8.20 ms, TE = 3.79 ms, TI = 900 ms), with a 256×256 image matrix, 1×1×1 mm³ voxel size, and 117 echo train length. The DW images were acquired [14] using a single-shot spin-echo echo-planar imaging (EPI) sequence (TR = 1815.34 ms, TE = 95.55 ms, slice thickness = 2.5 mm, acquisition matrix = 94×94, reconstruction matrix = 96×96). A multi-shell multi-tissue diffusion scheme was used, including 30 directions at b = 2000 s/mm², 30 directions at b = 1000 s/mm², and 6 directions at b = 500 s/mm², along with a b = 0 s/mm² image (b0). An additional b0 image with reversed phase-encoding (PE) direction was acquired.

B. DWI preprocessing and whole brain tractography

Diffusion weighted image data were processed using an open-source software, MRtrix3 (https://www.mrtrix.org/) and FSL (https://fsl.fmrib.ox.ac.uk/fsl/docs/#/), following Zhang's review processing steps [12]. For each DWI, noise reduction and Gibb's ringing artefacts removal were performed. Then b0 images acquired in both PE and reversed PE direction were used for EPI-distortion, B0-field inhomogeneity, eddy-current and movement distortion correction. The direction of the white matter fibers in each voxel was obtained using multi-shell multi-tissue constrained spherical deconvolution. Then a probabilistic algorithm was employed to identify white matter tracts together with the anatomically constrained tractography.

Finally, to address the non-quantitative nature of diffusion MRI tractography, we applied the SIFT2 method. This approach refines streamline reconstructions by assigning an appropriate cross-sectional area multiplier to each streamline, allowing for biologically accurate measures of fiber connectivity while preserving the complete tractogram.

C. Structural connectome

For each subject a whole-brain connectome was generated based on the HCP MMP1 atlas [15], with 180 parcels for each hemisphere. The parcellation was performed using FreeSurfer (https://surfer.nmr.mgh.harvard.edu/). Through MRtrix3 the structural connectivity (SC) matrix of each subject was computed. Each value of the matrix represents the number of streamlines connecting the two nodes, weighted these values by the inverse of the volumes of the two parcels, to compensate for variances in node size across the dataset [16].

The SC matrix allows to gain quantitative information on the strength of connection between cortical regions. To compare the SC matrix across subjects, values were normalized between 0 and 1. The workflow for the connectome construction is showed in Fig. 1.

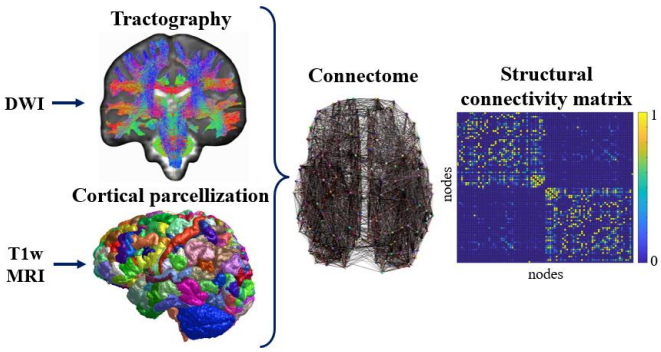

Fig. 1: Workflow of the extraction of the structural connectome from DWI and T1w MRI for each subject using MRtrix3, FSL and FreeSurfer.

D. Anatomical modelling

Simulations were performed on subject-specific head models, reconstructed through the Sim4Life *eHead40* function in a voxel-based format by the segmentation of T1w MRI. Up to forty different tissues were distinguished. To balance tissue reconstruction accuracy with computation time, the output voxel spacing was set to 0.3 mm.

E. EM characterization and simulation settings

tDCS simulations were performed using the electromagnetic commercial software Sim4Life. In the near DC frequency range relevant to tDCS, the quasi-static Laplace equation (1) is considered as a valid approximation [17] to determine the electric potential distribution (φ) inside the human models due to stimulation:

$$\nabla(\sigma\nabla\varphi) = 0 \quad (1)$$

where σ (S/m) is the electrical conductivity of the tissues. For electrically anisotropic materials such as white matter the conductivity can be represented by a symmetric 3 × 3 tensor.

The EF distribution in each point of the conductive medium was obtained by means of the equation (2):

$$\boldsymbol{EF} = -\nabla\varphi \quad (2)$$

For each participant two simulations were performed: one considering all tissues isotropic and another one including white matter anisotropy ("NoDTI-Sim", "DTI-Sim").

The conductivities of the head tissues were assigned according to the data collected in the IT'IS low-frequency tissue properties database [18]. The isotropic electrical properties of the tissues mostly involved in tDCS are: σ_{skin} = 0.148 S/m, σ_{fat} = 0.078 S/m, σ_{CSF} = 1.879 S/m, $\sigma_{grey\ matter}$ = 0.419 S/m, $\sigma_{white\ matter}$ = 0.348 S/m, $\sigma_{bone\ cancellous}$ = 0.08 S/m, $\sigma_{bone\ cortical}$ = 0.0063 S/m.

The white matter tissue anisotropy was assigned based on the hypothesis that the orientation of the diffusion tensor major eigenvector is generally assumed to be parallel to the local fibers [19]. After preprocessing in MRtrix3, the DTI data were converted into a format supported by Sim4Life, through *s4l-dti*, a python package (https://github.com/dyollb/s4l-dti) enabling the assignment of anisotropic inhomogeneous conductivity maps in tissue models.

In all simulations electrodes were placed according to the 10-10 EEG system: the anode over the posterior parietal cortex (P2) and the cathode over the contralateral supraorbital area (AF3). The electrodes were modelled as rectangular pads (3 × 3 cm^2, 5 × 5 cm^2 for anode and cathode, respectively) of 1 mm thick copper (σ = 5.9 × 10^7 S/m) placed above a conductive sponge with the same dimensions (σ = 1.4 S/m [20]) and thickness of 5 mm. The modelling was done through SimNIBS (https://simnibs.github.io/). The two electrodes were set to a fixed potential (+/- 1V) and the results were later scaled to simulate a current of 0.75 mA, consistent to [21]. The computational domain was truncated at the neck level to reduce computational cost. A non-uniform hexahedral mesh (min/max resolution= 0.5/2 mm) was used for discretization, resulting in approximately 110 million cells.

F. Analysed quantities

Structural connectivity. The structural connectivity matrix was extracted from each subject's DWI. Subsequently, the following metrics were evaluated:

- Adjusted interindividual variability in brain connectomes. It was evaluated using the following formula (3):

$$Var(i) = 1 - E\left[corr\left(SC_i(s_p), SC_i(s_q)\right)\right] \quad (3)$$

  where SC_i is the structural connectivity between region i and all the other regions, s_q and s_p refers to subjects (p,q = 1,2,…,N p≠q) [11].
- Strength of connection (SC values) between the cortical area under the anode and: parcels across the entire atlas;

parcels within the left hemisphere only.

The cortical area under the anode was considered as the one composed by the following parcels of the HCP MMP1 atlas all in the right hemisphere (R_): 7m, 5m, 5L, 7AL, 7Am, 7PL, 7PC, LIPv, VIP, MIP, AIP.

EF distribution. Once the most connected parcels to the anode were found, we chose to extract EF distribution on both the whole white matter and on four specific regions of interest (ROIs), as shown in Fig. 2.

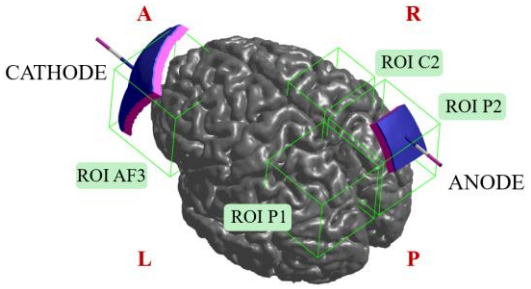

Fig. 2: Anode and cathode placement over P2 and AF3 respectively; region of interest boxes (sensors) from which EF distributions were extracted.

To investigate the intersubject variability in structural connectome and the influence of white matter anisotropy in the amplitude, spread, and orientation of the EF, the following metrics were extracted or computed:

- **MaxEF**: Peak amplitude of the EF distribution in white matter across all ROIs.
- **MaxDiff**: Peak difference in EF distribution between NoDTI-Sim and DTI-Sim.
- **RE (Residual Error)**: Quantifies the relative difference between EF distributions [11].
- **V50, V70, V80**: percentage volume of white matter where the EF amplitude was greater than the 50%, 70%, 80% of the MaxEF for each ROI. They assess the effect of DTI-based modelling on tDCS focusing capability.
- **MaxAlpha**: Peak of the angle difference between EF orientations in **NoDTI-Sim** and **DTI-Sim** (4) [22]:

$$Alpha_{(DTI-NoDTI)}(i) = \cos^{-1}\left(\frac{\overrightarrow{EF}_{DTI}(i)\cdot\overrightarrow{EF}_{NoDTI}(i)}{\|\overrightarrow{EF}_{DTI}(i)\|\|\overrightarrow{EF}_{NoDTI}(i)\|}\right) \quad (4)$$

MaxEF, MaxDiff, MaxAlpha are computed using the 99th percentile to filter spurious points due to staircase errors [22].

III. Results and Discussion

Structural connectivity. SC matrixes found (Fig. 1) are consistent with previous studies using probabilistic tractography [23]. The mean of the adjusted intersubject variability across all brain parcels is 18.6% ± 1.29%.

The highest variability, i.e. 19.4%, is reached in associative areas of the left hemisphere and in the right amygdala, while the lowest variability, i.e. 14.21%, is found in parcels of the visual cortex. This aligns with the findings of [7] which stated that SC shows greater variability in limbic regions while lower in unimodal sensorimotor regions.

The intersubject variability of connections between the parcels under the anode and all the other regions, is 18.81%. This result emphasizes the need to account for these differences when interpreting results for the specific stimulation setup used in our study. Despite the observed variability, we identified two key regions - one homolateral and one contralateral to the anode - comprising the parcels with the strongest structural connections to the anode. In the right hemisphere, the most strongly connected parcels are in the upper part of the precentral and postcentral cortex, beneath the C2 position in the 10-10 EEG reference system: R_1, 2, 3b, 4, and 6mp. In the left hemisphere, the most connected parcels correspond to the homologous regions of those under the anode, positioned near the P1 reference point. This rationale guided the placement of EF sensors in the simulations, centring them in P2, C2, and P1. Additionally, AF3 was included as it corresponds to the cathode placement, despite the absence of direct structural connections between its parcels and those under the anode.

Impact of DTI in EF distribution. Fig. 3 shows the differences in EF distribution when white matter anisotropy is either included or neglected in the simulations. A clear local EF enhancement (e.g., in corpus callosum) is observed in regions where the current is forced to cross fibre pathways in an orthogonal projection. This effect arises due to a reduction in conductivity along these pathways [10].

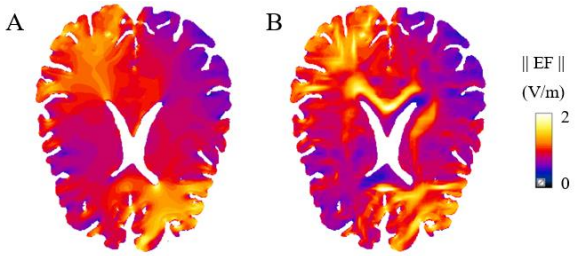

Fig. 3: EF distribution on an axial slice of the white and grey matter A) no DTI simulation; B) DTI simulation.

Table I quantifies the differences in EF distribution with and without white matter anisotropy. Notably, the inclusion of DTI reveals higher EF values, with the largest EF difference in C2 and P2 (under the anode). Specifically, the EF difference between the two models reaches 35% relative to the peak EF in the isotropic simulation. These results highlight the significant impact of neglecting white matter anisotropy, leading to potential errors in estimating the EF distribution.

To systematically assess this discrepancy, we computed the RE for each ROI (AF3, C2, P1, P2). The values obtained - 0.152, 0.145, 0.111, and 0.138, respectively -indicate that the error remains consistently above 10% across all ROIs.

Impact of DTI on EF Orientation and Spread. Beyond magnitude differences, the directionality of the EF is also affected by neglecting anisotropy. Our analysis reveals that ignoring DTI-based anisotropy introduces an orientation error of approximately 30 degrees. This is particularly critical for microscopic neural analysis, where even subtle changes in EF orientation can influence subthreshold neuronal responses.

The spread of the EF in each ROI was further analysed using V50, V70, and V80 metrics. Across the entire white matter volume, we observed a greater EF focalization when DTI is included: V50 - 8.6% (DTI) vs. 10.8% (NoDTI); V70 - 2.5% vs. 3.5%; V80 - 1.04% vs. 1.52%.

These results indicate that incorporating white matter anisotropy leads to a more localized EF distribution. When examining individual ROIs, this focalization effect is most evident in C2, which is the region most structurally connected

to the anode. Despite reaching the highest MaxEF, C2 exhibits also the strongest EF focused effect.

Linking EF distribution to structural connectivity. These findings highlight the importance of incorporating SC into tDCS protocol design to enhance personalization. Our study further demonstrates that SC substantially influences EF distribution, prompting the investigation of this relationship within the SC matrix.

TABLE I: EF DISTRIBUTION IN DTI AND NO DTI SIMULATIONS

ROI	*MaxEF (mV/m)*		*MaxDiff (mV/m)*	*MaxAngle (deg)*
	NoDTI	*DTI*		
AF3	194 ± 21	182 ± 22	45.6 ± 17	26.9 ± 3.3
C2	192 ± 21	233 ± 34	81.8 ± 22	28.9 ± 3.1
P1	144 ± 15	145 ± 14	40.2 ± 8	28.5 ± 4.0
P2	219 ± 26	226 ± 39	76.7 ± 22	27.6 ± 3.9

Mean and standard deviation for MaxEF in NoDTI-Sim and DTI-Sim; MaxDiff and MaxAngle.

Our preliminary analysis revealed a positive correlation ($r = 0.56$, $p = 0.02$) between the strength of connections between ROI P2 and C2 and V80, indicating that regions with stronger structural connections experience a more focused EF. These results open the way for future investigations into how connectivity-informed tDCS protocols could be optimized for personalized neuromodulation strategies.

IV. CONCLUSION

Our results underscore the importance of integrating individualized protocols that account for white matter connectivity during tDCS optimization.

Metrics reflecting the strength of connectivity between the anode with the other cortical areas should be considered to better explain the variability in the EF distributions.

DTI inclusion leads to both higher EF intensities and increased EF focality, mostly in areas more structurally connected to the anode. This highlights the potential for incorporating white matter connectivity estimates into tDCS protocol design to achieve more targeted and effective neuromodulation.

ACKNOWLEDGEMENT

The authors would like to thank ZMT Zurich MedTech AG (www.zmt.swiss) for having provided the simulation software SIM4Life. This study was supported by the Italian Ministry of University and Research (MUR) under the PRIN 2022 project 2022CYRMAT titled “A multidisciplinary approach for the definition of the stimulation dose for transcranial electrical stimulation tuned by individual brain variability - PROMETEO”.

REFERENCES

[1] A. Priori, “Brain polarization in humans: a reappraisal of an old tool for prolonged non-invasive modulation of brain excitability,” Clinical Neurophysiology, vol. 114, no. 4, pp. 589–595, Apr. 2003, doi: 10.1016/S1388-2457(02)00437-6.

[2] A. Liu et al., “Immediate neurophysiological effects of transcranial electrical stimulation,” Nat Commun, vol. 9, no. 1, p. 5092, Nov. 2018, doi: 10.1038/s41467-018-07233-7.

[3] F. Ferreri et al., “Age-related changes of cortical excitability and connectivity in healthy humans: non-invasive evaluation of sensorimotor network by means of TMS-EEG,” Neuroscience, vol. 357, pp. 255–263, Aug. 2017, doi: 10.1016/j.neuroscience.2017.06.014.

[4] M.-F. Kuo, W. Paulus, and M. A. Nitsche, “Therapeutic effects of non-invasive brain stimulation with direct currents (tDCS) in neuropsychiatric diseases,” Neuroimage, vol. 85, pp. 948–960, Jan. 2014, doi: 10.1016/j.neuroimage.2013.05.117.

[5] I. Laakso, M. Mikkonen, S. Koyama, A. Hirata, and S. Tanaka, “Can electric fields explain inter-individual variability in transcranial direct current stimulation of the motor cortex?,” Sci Rep, vol. 9, no. 1, Dec. 2019, doi: 10.1038/s41598-018-37226-x.

[6] A. Vergallito, S. Feroldi, A. Pisoni, and L. J. R. Lauro, “Inter-Individual Variability in tDCS Effects: A Narrative Review on the Contribution of Stable, Variable, and Contextual Factors,” May 01, 2022, MDPI. doi: 10.3390/brainsci12050522.

[7] W. Huang (黄伟杰) et al., “Individual Variability in the Structural Connectivity Architecture of the Human Brain,” The Journal of Neuroscience, vol. 45, no. 5, p. e2139232024, Jan. 2025, doi: 10.1523/JNEUROSCI.2139-23.2024.

[8] V. Baliyan, C. J. Das, R. Sharma, and A. K. Gupta, “Diffusion weighted imaging: Technique and applications,” World J Radiol, vol. 8, no. 9, p. 785, 2016, doi: 10.4329/wjr.v8.i9.785.

[9] P. C. Miranda, M. A. Callejón-Leblic, R. Salvador, and G. Ruffini, “Realistic modeling of transcranial current stimulation: The electric field in the brain,” Dec. 01, 2018, Elsevier B.V. doi: 10.1016/j.cobme.2018.09.002.

[10] S. Shahid, P. Wen, and T. Ahfock, “Assessment of electric field distribution in anisotropic cortical and subcortical regions under the influence of tDCS,” Bioelectromagnetics, vol. 35, no. 1, pp. 41–57, 2014, doi: 10.1002/bem.21814.

[11] H. S. Suh, W. H. Lee, and T. S. Kim, “Influence of anisotropic conductivity in the skull and white matter on transcranial direct current stimulation via an anatomically realistic finite element head model,” Phys Med Biol, vol. 57, no. 21, pp. 6961–6980, Nov. 2012, doi: 10.1088/0031-9155/57/21/6961.

[12] F. Zhang et al., “Quantitative mapping of the brain’s structural connectivity using diffusion MRI tractography: A review,” Neuroimage, vol. 249, Apr. 2022, doi: 10.1016/j.neuroimage.2021.118870.

[13] R. E. Smith, D. Raffelt, J.-D. Tournierc, and A. Connelly, “Quantitative streamlines tractography: methods and inter-subject normalisation,” Aperture Neuro, pp. 1–25, Sep. 2022, doi: 10.52294/ApertureNeuro.2022.2.NEOD9565.

[14] J. -Donald Tournier, F. Calamante, and A. Connelly, “Determination of the appropriate b value and number of gradient directions for high-angular-resolution diffusion-weighted imaging,” NMR Biomed, vol. 26, no. 12, pp. 1775–1786, Dec. 2013, doi: 10.1002/nbm.3017.

[15] M. F. Glasser et al., “A multi-modal parcellation of human cerebral cortex,” Nature, vol. 536, no. 7615, pp. 171–178, Aug. 2016, doi: 10.1038/nature18933.

[16] H. Byrne et al., “Hypothalamus Connectivity in Adolescent Myalgic Encephalomyelitis/Chronic Fatigue Syndrome,” J Neurosci Res, vol. 102, no. 10, p. e25392, Oct. 2024, doi: 10.1002/jnr.25392.

[17] M. Parazzini, S. Fiocchi, I. Liorni, and P. Ravazzani, “Effect of the Interindividual Variability on Computational Modeling of Transcranial Direct Current Stimulation,” Comput Intell Neurosci, vol. 2015, pp. 1–9, 2015, doi: 10.1155/2015/963293.

[18] P. Hasgall et al., “‘IT’IS Database for thermal and electromagnetic parameters of biological tissues,’” Version 4.1. Accessed: Jun. 05, 2024. [Online]. Available: itis.swiss/database

[19] P. J. Basser, J. Mattiello, and D. LeBihan, “MR diffusion tensor spectroscopy and imaging,” Biophys J, vol. 66, no. 1, pp. 259–267, Jan. 1994, doi: 10.1016/S0006-3495(94)80775-1.

[20] A. Datta, J. M. Baker, M. Bikson, and J. Fridriksson, “Individualized model predicts brain current flow during transcranial direct-current stimulation treatment in responsive stroke patient,” Brain Stimul, vol. 4, no. 3, pp. 169–174, Jul. 2011, doi: 10.1016/j.brs.2010.11.001.

[21] L. J. Romero Lauro et al., “TDCS increases cortical excitability: Direct evidence from TMS-EEG,” Cortex, vol. 58, pp. 99–111, 2014, doi: 10.1016/j.cortex.2014.05.003.

[22] M. Parazzini et al., “A computational model of the electric field distribution due to regional personalized or nonpersonalized electrodes to select transcranial electric stimulation target,” IEEE Trans Biomed Eng, vol. 64, no. 1, pp. 184–195, Jan. 2017, doi: 10.1109/TBME.2016.2553177.

[23] S. Y. Tsai, “Reproducibility of structural brain connectivity and network metrics using probabilistic diffusion tractography,” Sci Rep, vol. 8, no. 1, Dec. 2018, doi: 10.1038/s41598-018-29943-0.